Ground state of the Frenkel-Kontorova model with a transverse degree of freedom

O. M. Braun
Institute of Physics, Ukrainian Academy of Sciences, 46 Science Avenue, Kiev, UA-252022, Ukraine

M. Peyrard
Laboratoire de Physique, Ecole Normale Supérieure de Lyon, 46 Allée d'Italie, 69364 Lyon Cédex 07, France
(Received 14 December 1994)

We study the ground state of a generalized Frenkel-Kontorova model with a transverse degree of freedom. The model describes a lattice of atoms with a fixed concentration, interacting by long-range repulsive forces, which is submitted to a two-dimensional substrate potential periodic (sinusoidal) in one direction and symmetric (parabolic) or asymmetric (Toda-like) in the transverse direction. When the magnitude of the interatomic repulsion increases, the ground state of the model undergoes a series of bifurcations. In particular, the first bifurcation leads to a zigzag ground state and results in drastic change of system properties, including a cusp in the average elastic constant. For incommensurate cases, the bifurcation can interplay with the Aubry transition from a pinned to a sliding state. A reentrant pinned state has, for instance, been found. The nature (continuous or discontinuous) of the next bifurcations depends on the symmetry of the substrate potential in the transverse direction. Finally, we discuss briefly the applicability of the model to describe conductivity of superionic conductors, surface diffusion, and crystal growth.

PACS number(s): 46.10.+z, 63.20.Ry, 03.40.Kf

I. INTRODUCTION

Various nonlinear phenomena in solid state physics can be described by a model where a chain of interacting particles is placed in a "channel." The atomic chain is subjected to a two- or three-dimensional external potential, which is periodic in one direction and unbounded (for example, parabolic) in transverse directions so that the atoms are confined transversally. Such a model arises when we can pick out a one-dimensional subsystem from the whole system and consider the rest of the system as the source of an external (substrate) potential and, at the same time, as a thermal bath supporting an energy exchange with the subsystem of interest. Typical examples are (i) *superionic conductors* [1], where an anisotropic crystalline structure forms channels along which ions can easily move, (ii) *crowdions* [2], which describe extra atoms or vacancies inserted into a closely packed atomic row in a metal with an ideal crystal lattice (in many cases the crystalline potential is such that the atoms can move easily only along the direction of the row); (iii) *submonolayer films* [3] of atoms adsorbed on furrowed or stepped crystal surfaces, where the adsorbed atoms (adatoms) in a given furrow or at a step move easily along the direction of the furrow or step and form a quasi-one-dimensional system, while the surface atoms and other adatoms produce an effective external potential (such a model may be also used to describe surface reconstruction and crystal growth); and (iv) *hydrogen-bonded systems* along channels in biomembranes [4], where protons are the mobile particles, while a heavy-ion lattice of oxygen atoms produces an external potential.

If we ignore atomic displacements in transverse directions and allow the atoms to move only along the direction of the chain, the model reduces to a variant of the well-known Frenkel-Kontorova (FK) model. Introduced first to describe the structure of a crystal lattice near a core of a dislocation [5], the FK model was then successfully used to describe, besides the examples mentioned above, nonlinear phenomena such as dislocation dynamics, charge-density waves, ferroelectric domain walls, magnetically ordered structures, and commensurate-incommensurate transitions. The standard FK model, where the substrate potential is assumed to be sinusoidal and the interatomic interaction is restricted to the interaction of nearest neighbors by harmonic forces only, was then generalized for a nonsinusoidal substrate and a nonharmonic interaction (see the review paper [6] for other generalizations and applications of the FK model). All these studies, however, have been restricted to one spatial dimension.

There are few papers devoted to two-dimensional (2D) generalizations of the FK model. The standard FK model can be extended to two dimensions in two ways. The simplest approach assumes that the atoms form a 2D lattice but the field variable has still a scalar nature, i.e., the atoms can move in a single direction only. This is the *scalar* 2D FK model [7]. An infinite system of parallel FK chains when an interaction between the chains is taken into account is a physical realization of this model. The second approach leads to the *vector* 2D FK model, which describes a 2D array of interacting atoms mobile in both directions and subjected to a 2D external potential that is periodic in both directions [8]. The analysis of vector models is difficult and results can only be obtained by computer simulation. Moreover, the studies [8] gener-

ally take into account the interaction of a small number of neighbors only and assume that the interaction is harmonic, as in the standard FK model. But these "ball and spring" models are only rigorous if mutual displacements of neighboring atoms are small compared with the lattice constant. In other words, within the ball and spring model we must artificially neglect configurations where atomic displacements from the ideal lattice are too large.

When we consider a more realistic vector 2D FK model, we lose the main advantage of the one-dimensional model in which atoms are always strictly ordered and therefore can be labeled in such a way that atom i always has atoms $i \pm 1$ nearest neighbors. In a realistic 2D model the sequential order of the atoms can be changed by going through the second dimension. Therefore, a rigorous 2D model must take into account the interaction between *all* the atoms in the system. As a result, the system behavior becomes very rich and complicated even for a single atomic row picked out from the whole 2D lattice and subjected to the 2D substrate potential. We consider such a model in the present work. This model may be considered as the simplest approximation for an *anisotropic* vector 2D FK model where we could expect that a small interaction between the nearest-neighboring rows does not modify significantly the properties of the system. On the other hand, the model may be considered as a first step in studying the *isotropic* 2D FK model. The main difference with the standard FK model in which particles move along the x direction is that here they are allowed to move along x and y. A single-well substrate potential is imposed along the y direction and a *repulsive* particle-particle interaction is used.

The FK model with a transverse degree of freedom was proposed in [9]. It was shown that the trivial ground state (TGS) Fig. 1(a) becomes unstable and evolves into a zigzag ground state (ZGS) Fig. 1(b) when the repulsion between atoms increases above a certain threshold value. Close to the transition point, as well as above this point, properties of the FK model are deeply changed. In particular, the kink-antikink symmetry is violated even for a harmonic interaction between the atoms. However, this previous work [9] considers only the simplest case, when the number of atoms N coincides with the number of minima of the external potential M so that the dimensionless concentration $\theta = N/M$ (the so-called coverage in surface physics) is equal to one. Moreover, the interatomic interaction was restricted to the interaction of nearest and next nearest neighbors, so that only the TGS and the ZGS could be studied.

The present work generalizes the previous studies [9] in two directions. First, we investigate the behavior of the model for arbitrary concentration $\theta \neq 1$ (but $\theta \leq 1$) including incommensurate cases when θ is an irrational number and the standard FK model exhibits the Aubry transition. We show in particular how the zigzag ground state found previously can compete with the Aubry transition or even cause multiple Aubry transitions.

Another different aspect of the present work is that we take into account the interaction of *all* atoms in the chain. This is not only of qualitative importance because the extended model can have a full sequence of bifurcation that was not possible with short-range interactions. The origin of these bifurcation can be understood easily from qualitative arguments. The zigzag configuration can be treated as consisting of two subchains, the upper subchain and the lower subchain. When the coupling between the subchains is small, for example, when transverse substrate potential is weak so that the distance between the subchains is large, the subchains can be considered as independent. So the same arguments that explained the first bifurcation to a zigzag state can be repeated and we can expect that each subchain can become unstable to a new zigzag instability splitting the system in new quasi-independent chains. We show, however, that the real scenario is more subtle than this simple picture, which seems to predict an infinite sequence of bifurcation. In particular, the symmetry of the transverse potential is very important. For a symmetric potential the instabilities of the two first subchains occur simultaneously. And because near an unstable point a system is very sensitive to perturbations, the weak interaction between the subchain has in fact a strong influence. This phenomenon would not occur for an asymmetric potential. This is why we consider here the two cases of a symmetric (parabolic) and a nonsymmetric (Toda) transverse potential.

The model that we study can have a very rich behavior and, as we discuss in Sec. VII, its study is not only of academic interest. We expect that some of these behaviors could be relevant for real systems, particularly for surface diffusion and crystal growth.

The paper is organized as follows. In Sec. II we introduce the model and describe the algorithm used in the numerical analysis. Section III is devoted to the TGS-ZGS transition for a rational concentration θ including situations corresponding to kink and antikink configurations. In Sec. IV we analyze an irrational θ case and show how the transverse degree of freedom modifies the Aubry transition. The second and further bifurcations are investigated in Sec.V for the symmetric model and in Sec. VI for the asymmetric Toda-like case. Finally, Sec. VII concludes the paper by a discussion of the possible application of the model to describe conductivity of superionic conductors, surface diffusion, and crystal growth.

II. MODEL

Let us consider a chain of interacting atoms subjected to a 2D external substrate potential $V_s(\mathbf{r})$ with $\mathbf{r} \equiv (x, y)$. We assume that $V_s(\mathbf{r})$ is the sum of two terms

$$V_s(\mathbf{r}) = V_x(x) + V_y(y), \tag{1}$$

where $V_x(x)$ is a periodic potential along the chain, which is assumed to be sinusoidal,

$$V_x(x) = \frac{1}{2}\epsilon_s[1 - \cos(2\pi x/a_s)], \tag{2}$$

and $V_y(y)$ is a confining potential in the transverse di-

rection, which is taken to be parabolic for the symmetric case

$$V_y(y) = \frac{1}{2} m_a \omega_{0y}^2 y^2. \tag{3}$$

Here ϵ_s is the amplitude and a_s is the period of the substrate potential, m_a is the atomic mass, and ω_{0y} is the frequency of a single-atom vibration in the transverse direction. The limit $\omega_{0y} \to \infty$ corresponds to the standard FK model. It is convenient to use units such that $m_a = 1$, $\epsilon_s = 2$, and $a_s = 2\pi$ so that the frequency of longitudinal vibrations $\omega_{0x} = (\epsilon_s/2m_a)^{\frac{1}{2}}(2\pi/a_s)$ is equal to 1.

For noninteracting atoms, the x and the y degrees of freedom are decoupled due to the simple form chosen for the substrate potential in Eq. (1). However, the interatomic interaction couples the degrees of freedom. As long as the atoms use only an attractive branch of the interaction potential, static properties of the model are equivalent to those of the standard FK model (but the dynamics is modified). In a number of physical systems, however, the interatomic interaction is repulsive or has at least a repulsive branch. It can be due to Coulomb repulsion between ions in superionic conductors [1] or between protons in hydrogen-bonded molecules [4], or to Coulomb or dipole-dipole repulsion of atoms adsorbed on semiconductor or metal surfaces [10]. The aim of the present work is to find the ground-state (GS) atomic configuration and to study its properties for the case of a repulsion between the atoms. We assume a Coulomb repulsion

$$V(r) = V_0/r, \tag{4}$$

where V_0 characterizes the amplitude of repulsion. Note that qualitative results do not depend on the specific form of $V(r)$ provided that the repulsion is concave, i.e., if $V(r)$ decreases monotonically with increasing distance r between the atoms.

For repulsive interactions the boundary conditions are essential to determine the properties of the system because, with free boundaries, the system would tend to decrease its energy by expanding indefinitely. In a physical system, this is generally not possible and, for instance, for atoms adsorbed on a surface, the average density of atoms is imposed by the experimental conditions. We represent this situation by imposing a fixed density of atoms. The chain consists of N atoms distributed on the length $L = Ma_s = Na_A$, where M is the number of minima of $V_x(x)$ and a_A is the mean interatomic distance along the chain. Therefore the system is characterized by the dimensionless concentration $\theta = N/M = a_s/a_A$, which is kept fixed in the limit $N,M \to \infty$. The total potential energy of the system is

$$U = \sum_{i=1}^{N} \Bigg[V_s(\mathbf{r}_i) + \frac{1}{2} \sum_{i'=1}^{N^*} [V(|\, \mathbf{r}_i - \mathbf{r}_{i+i'} \,|) + V(|\, \mathbf{r}_i - \mathbf{r}_{i-i'} \,|)] \Bigg], \tag{5}$$

where the index i labels the atoms and the limit $N, N^* \to \infty$ is assumed. The GS configuration corresponds to the absolute minimum of U. So to find the GS atomic coordinates $\{\mathbf{r}_i^{(0)}\} \equiv \{x_i^{(0)}, y_i^{(0)}\}$, we look for static configurations by solving the set of equations $\partial U/\partial x_i = 0$, $\partial U/\partial y_i = 0$, $i = 1, \ldots, N$, and then select the GS configuration that gives the absolute minimum of U.

When the GS coordinates are known, we can calculate the GS phonon spectrum. The spectrum is determined by the eigenfrequencies of the elastic matrix $\mathbf{A}$ introduced as [11]

$$A_{ii}^{\alpha\alpha'} = \left[\frac{\partial^2 V_s(\mathbf{r}_i)}{\partial u_i^\alpha \partial u_i^{\alpha'}} + \sum_{i'(i' \neq i)} \frac{\partial^2 V(|\, \mathbf{r}_i - \mathbf{r}_{i'} \,|)}{\partial u_i^\alpha \partial u_{i'}^{\alpha'}} \right]_{\text{all } \mathbf{u}=0}, \tag{6}$$

$$A_{ii'(i \neq i')}^{\alpha\alpha'} = \left[\frac{\partial^2 V(|\, \mathbf{r}_i - \mathbf{r}_{i'} \,|)}{\partial u_i^\alpha \partial u_{i'}^{\alpha'}} \right]_{\text{all } \mathbf{u}=0},$$

where the greek indices correspond to Cartesian coordinates ($\alpha, \alpha' = x$ or y), and the vector $\mathbf{u}_i = \mathbf{r}_i - \mathbf{r}_i^{(0)}$ describes the displacement of the ith atom from its equilibrium position. In particular, for the sinusoidal potential (2) and the Coulomb repulsion (4) we have

$$A_{ii}^{xx} = \cos x_i^{(0)} + \sum_{i'(i' \neq i)} A_{ii'}^{xx}, \tag{7a}$$

$$A_{ii}^{yy} = \omega_{0y}^2 + \sum_{i'(i' \neq i)} A_{ii'}^{yy}, \tag{7b}$$

$$A_{ii}^{xy} = \sum_{i'(i' \neq i)} A_{ii'}^{xy}, \tag{7c}$$

with

$$A_{ii'(i \neq i')}^{xx} = -V_0(2x_{ii'}^2 - y_{ii'}^2)/r_{ii'}^5, \tag{7d}$$

$$A_{ii'(i \neq i')}^{yy} = -V_0(2y_{ii'}^2 - x_{ii'}^2)/r_{ii'}^5, \tag{7e}$$

$$A_{ii'(i \neq i')}^{xy} = -3V_0 x_{ii'} y_{ii'}/r_{ii'}^5, \tag{7f}$$

where $x_{ii'} = x_i^{(0)} - x_{i'}^{(0)}$, $y_{ii'} = y_i^{(0)} - y_{i'}^{(0)}$, and $r_{ii'} = (x_{ii'}^2 + y_{ii'}^2)^{1/2}$. If the dimensionless concentration θ is rational and the GS configuration is commensurate, the atomic structure is periodic so that it is convenient to take the Fourier transform

$$D_{mm'}^{\alpha\alpha'}(k) = \sum_{l=-\infty}^{\infty} A_{0,m;\,l,m'}^{\alpha\alpha'} \exp(ikla). \tag{8}$$

Here a is the period of the GS structure and the atomic index i is split into two subindices $i = (l, m)$, where the index l labels the elementary cells while $m = 1, \ldots, s$ denote the atoms within the cell. For each momentum k ($|\, k \,| \leq \pi/a$), $\mathbf{D}(k)$ is a $2s \times 2s$ square matrix and the phonon spectrum consists of $2s$ branches labeled by an index j. The frequencies $\omega_j(k)$ are determined by the eigenequation

$$\det\left[\omega^2(k)\mathbf{1} - \mathbf{D}(k)\right] = 0. \tag{9}$$

For a stable configuration all eigenfrequencies must be positive. When, for some model parameters, one of the frequencies vanishes $\omega_j(k^*) = 0$, the corresponding configuration becomes unstable and evolves into a new configuration with the period $a^* = \pi/k^*$. The eigenvector associated with the vanishing frequency helps to find the new GS. This scenario corresponds to a continuous (second-order) phase transition. Moreover, the model may also exhibit discontinuous (first-order) phase transitions when a model parameter (e.g., V_0) is changed. They occur when the energy of a metastable configuration becomes equal to the energy of the GS configuration at a transition point $V_0 = V_{\rm bif}^{(m)}$; beyond this point the metastable and the GS configurations are exchanged.

Investigations of the standard FK model show [6] that the dimensionless elastic constant $g_{\rm FK} = (a_s^2/2\pi^2\epsilon_s)V''(a_A)$ plays a central role. For instance, the elastic constant determines the width of the topological defect (kink), which can be created by moving one-half of the FK chain by one lattice spacing. This defect corresponds to a dislocation in the lattice. When the elastic constant is large, it spreads over many sites, while it becomes narrow for small elastic coupling. For the standard FK model, the limit $g_{\rm FK} \to \infty$ corresponds to the exactly integrable sine-Gordon model. The parameter $g_{\rm FK}$ characterizes discreteness effects. In our 2D model, the average elastic constant g, defined by

$$g = \frac{1}{N}\sum_{i=1}^{N} g_i\,, \tag{10}$$

with

$$g_i = \frac{1}{2}\sum_{i'=1}^{N^*}\left[\frac{\partial^2}{\partial x_i^2}[V(|\,\mathbf{r}_i - \mathbf{r}_{i+i'}\,|) + V(|\,\mathbf{r}_i - \mathbf{r}_{i-i'}\,|)]\right]_{\text{all } \mathbf{u}=0}, \tag{11}$$

plays a similar role. For the standard FK model g, defined by Eqs. (10) and (11), coincides with $g_{\rm FK}$.

Most of the results of the present work have been obtained from a numerical analysis using the methods described in [12,13]. Namely, we consider a finite system of N atoms and fix the concentration θ by imposing periodic boundary conditions. To avoid artificially introduced topological defects, the value of N must be adapted to the structure of the GS, i.e., N has to be a multiple of the number of atoms in the GS elementary cell. For example, for the ZGS N must be even. Then we choose an appropriate initial atomic configuration and allow the system to relax to a nearest minimum of U. Starting from different initial configurations, we may converge to different final configurations and then we have to select the configuration that gives the absolute minimum of U. For the initial configurations we take uniform symmetric configurations obtained by cutting out stripes of different width from a hexagonal lattice as shown in Fig. 1. In order to generate an initial configuration with a given value of the concentration θ, we have to choose the constant of the hexagonal lattice appropriately. This choice of initial configurations is motivated by the fact that, in the absence of external corrugation, i.e., for the case $\epsilon_s = 0$, these configurations define the sequence of the GS configurations when the amplitude V_0 of interatomic repulsion increases.

The relaxation procedure uses Langevin equations

$$\frac{d^2x_i}{dt^2} + \eta\frac{dx_i}{dt} + \frac{\partial U}{\partial x_i} = \delta F_x(t), \tag{12a}$$

$$\frac{d^2y_i}{dt^2} + \eta\frac{dy_i}{dt} + \frac{\partial U}{\partial y_i} = \delta F_y(t), \tag{12b}$$

where η is the viscous friction coefficient and $\delta F_{x,y}(t)$ is a random force that corresponds to a fictitious temperature T. During the simulation T is decreased and it is set to zero after a time $t \sim 20\pi$, i.e., ten periods of oscillations in the potential V_x. This procedure helps to avoiding the trapping of the system in metastable configurations.

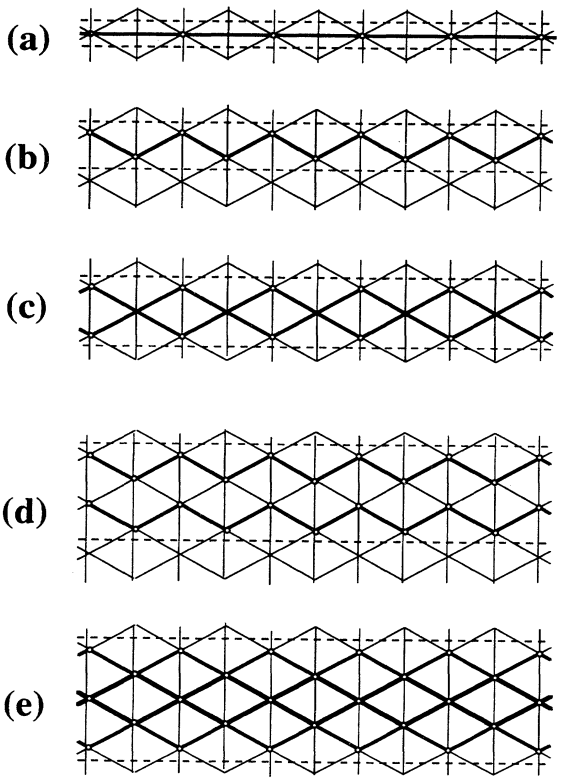

FIG. 1. Sequence of stripes cut out from a 2D hexagonal lattice showing the possible configurations of the atoms in the generalized FK model with a transverse degree of freedom. The horizontal axis is along the x direction. The vertical lines indicate the positions of the minima of the substrate potential. (a) Trivial ground state, where all atoms are situated on the line $y = 0$; (b) zigzag ground state; (c) rhomboid configurations, where two atoms are in the same valley of the periodic potential with different y coordinates; (d) double zigzag; and (e) hexagonal configurations.

The Langevin equations (12a) are solved for the time t_m needed for the system to approach sufficiently close to the final equilibrium state. The value of t_m is determined so that, at $t > t_m$, the atomic displacements Δx_i and Δy_i during an interval $\Delta t = 6\pi$ are bounded according to

$$\left(\sum_{i=1}^{N}\left[(\Delta x_i)^2 + (\Delta y_i)^2\right]\right)^{1/2} < \varepsilon ,$$

where ε determines the calculation accuracy (we use $\varepsilon = 10^{-5}$). The time t_m depends on the friction coefficient η; the shortest computation time is achieved with $\eta \simeq 1$.

Clearly in numerical calculations we can take into account only a finite number N^* of interacting neighbors. These neighbors cannot be simply chosen at the starting of the calculation because, in the 2D system, the sequence of the atoms can change. Therefore we have to use a standard procedure of molecular dynamics, i.e., select a cutoff distance L^* ($L^* \gg a_A$) and include in the calculation only atoms for which $r_{ii'} \leq L^*$. This condition determines the upper bound N^* of the summations in Eqs. (5) and (11).

In order to select the configuration with the lowest energy, we calculate the potential energy per atom E. Unfortunately, for the Coulomb interatomic repulsion the total energy of interaction depends on the cutoff distance L^* and diverges as $\ln L^*$ in the limit $L^* \to \infty$. To avoid this problem, we subtract from the total potential energy a constant equal to the repulsion energy in the uniform configuration with the atomic coordinates $x_i = ia_A$, $y_i = 0$. Thus each configuration is characterized by an energy

$$E = \frac{1}{N}\sum_{i=1}^{N}\left[V_s(\mathbf{r}_i^{(0)}) + \frac{1}{2}\sum_{i'=1}^{r_{i,i+i'}<L^*} V(r_{i,i+i'}) + \frac{1}{2}\sum_{i'=1}^{r_{i,i-i'}<L^*} V(r_{i,i-i'})\right] - S(N_m)V_0/a_A, \quad (13)$$

where $S(N_m) = 1 + \frac{1}{2} + \frac{1}{3} + \cdots + \frac{1}{N_m}$ and $N_m = \mathrm{int}(L^*/a_A)$.

III. THE FIRST BIFURCATION IN COMMENSURATE STATES

Let us start from the simplest case of the commensurate concentration $\theta = N/M = a_s/a_A = 1/q$ with an integer q, so that the average interatomic distance a_A is a multiple of the lattice constant a_s, $a_A = qa_s$. In this case, at small amplitude of interatomic repulsion, the GS is trivial (TGS) and all atoms are situated at the bottoms of the corresponding wells $x_i^{(0)} = ia_A$ and $y_i^{(0)} = 0$. The elementary cell of the system contains one atom only and the phonon spectrum consists of two branches [see Fig. 2(a)]. The first branch corresponds to motion along the x direction

$$\omega_1^2(k) = \omega_{0x}^2 + 2\sum_{l=1}^{\infty} V''(la_A)[1 - \cos(kla_A)] \quad (14)$$

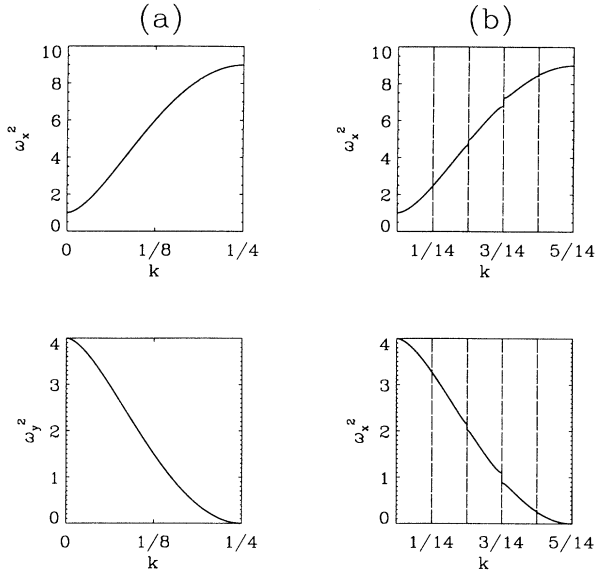

FIG. 2. Phonon spectrum of the commensurate trivial ground state for $\omega_{0y} = 2$ at $V_0 = V_{\mathrm{bif}}$. (a) $\theta = 1/2$ ($N^* = 64$) and $V_{\mathrm{bif}} = 1886$; (b) $\theta = 5/7$ ($N^* = 60$) and $V_{\mathrm{bif}} = 644.7$. In (b) we use the scheme of extended Brillouin zones.

and the second branch to motion along the y direction

$$\omega_2^2(k) = \omega_{0y}^2 + 2\sum_{l=1}^{\infty}[V'(la_A)/(la_A)][1 - \cos(kla_A)], \quad (15)$$

where $|\ k\ | \leq 1/2q$. Notice that the motions along the x and the y directions are decoupled.

For repulsive interatomic interactions, $V'(la_A) < 0$ so that, when the magnitude of the interatomic interaction increases, the frequency $\omega_2(k)$ decreases and reaches zero at some critical value $V_0 = V_{\mathrm{bif}}$. If the interatomic repulsion decreases monotonically with increasing r (i.e., if V' is always negative), the first instability arises at the momentum $k = \pm 1/2q$. The corresponding bifurcation value V_{bif} can be determined from the equation

$$\omega_{0y}^2 + 4\sum_{p=0}^{\infty}\frac{V'[(2p+1)a_A]}{(2p+1)a_A} = 0. \quad (16)$$

In particular, for the Coulomb repulsion (4) V_{bif} is equal to

$$V_{\mathrm{bif}} = \omega_{0y}^2 a_A^3/4C, \quad (17)$$

where $C \equiv \sum_{p=0}^{\infty}(2p+1)^{-3} = 1.05179\ldots$.

Thus, for any monotonically decreasing interatomic repulsion the first bifurcation always leads to a continuous transition from the trivial ground state of Fig. 1(a) to the zigzag ground state of Fig. 1(b) with atomic coordinates $x_i^{(0)} = ia_A$, $y_i^{(0)} = (-1)^i b$. The amplitude b of the transverse atomic shifts is determined by the equation

$$\omega_{0y}^2 + 4\sum_{l=0}^{\infty} V'(r_l)/r_l = 0, \quad r_l = [4b^2 + a_A^2(1+2l)^2]^{1/2}. \tag{18}$$

In the ZGS the value of the transverse splitting b increases with V_0, as shown in Fig. 3(a).

It will be convenient to use henceforth a dimensionless amplitude of interatomic repulsion defined as $v = d/a_A$, where $d = (4b^2 + a_A^2)^{1/2}$ is the distance between the nearest neighbors in the ZGS, so that $v_{\rm bif} = 1$. To obtain analytical estimates, let us consider the case of a Coulomb repulsion restricted to nearest and next nearest neighbors only. In this case the interaction is limited inside one cell

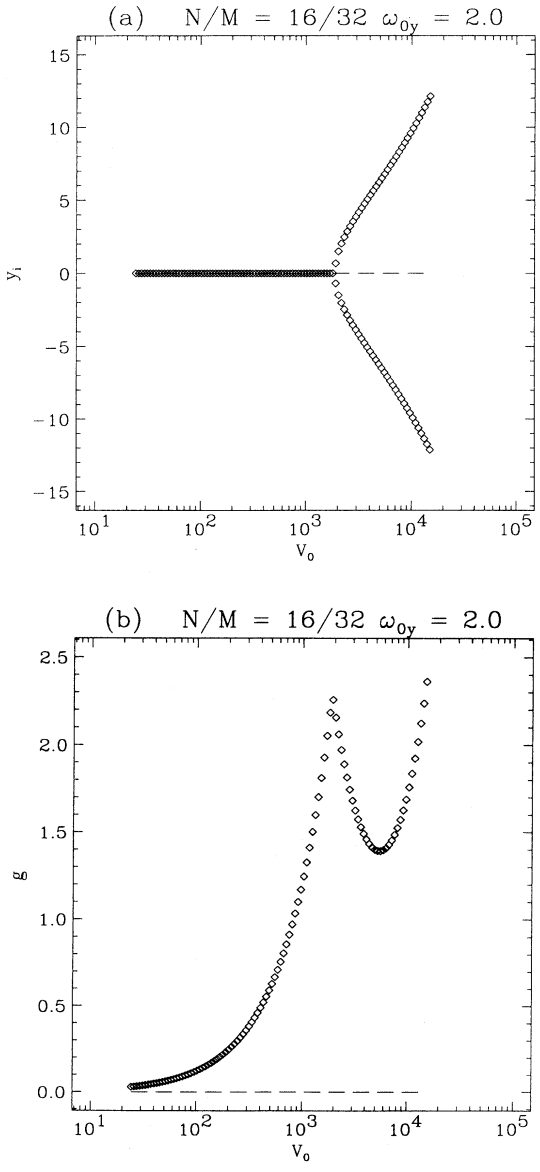

FIG. 3. (a) Transverse displacements y_i of the atoms and (b) average elastic constant g versus the amplitude of interatomic repulsion V_0 for $\theta = 1/2$ ($N = 16$, $M = 32$, and $N^* = 64$) and $\omega_{0y} = 2$.

of the ZGS so that only $p = 0$ has to be considered. From Eqs. (16)–(18) we get

$$V_{\rm bif} = \frac{1}{4}\omega_{0y}^2 a_A^3, \tag{19}$$

$$b = \frac{1}{2}\left[\left(4V_0/\omega_{0y}^2\right)^{2/3} - a_A^2\right]^{1/2}, \tag{20}$$

$$d = \left(4V_0/\omega_{0y}^2\right)^{1/3}, \tag{21}$$

and

$$v = \left(4V_0/\omega_{0y}^2 a_A^3\right)^{1/3}. \tag{22}$$

The average elastic constant (10) for the TGS is equal to

$$g_{\rm (TGS)} = \frac{9}{4}\frac{V_0}{a_A^3}, \tag{23}$$

while for the ZGS it is determined by the expression

$$g_{\rm (ZGS)} = \frac{1}{16}\omega_{0y}^2\left(v^3 + 12/v^2 - 4\right). \tag{24}$$

According to Eqs. (23) and (24), the elastic constant g for the TGS increases linearly with V_0 up to the value $g_{\rm bif} = 9\,\omega_{0y}^2/16$. But after the bifurcation g decreases, it reaches the local minimum $g_{\rm min} = 4.705\omega_{0y}^2/16 \sim 0.5 g_{\rm bif}$ at $v = 8^{1/5}$ and then rises again.

Figure 3 shows the numerical results for $\theta = \frac{1}{2}$ and $\omega_{0y} = 2$ ($N = 16$ and $M = 32$), taking into account the interaction of a large number of neighbors ($N^* = 64$). The results are in agreement with the predictions of the simple approach described above. Note that the cusp of the elastic constant g at the bifurcation point $V_{\rm bif}$ explains many remarkable properties of the model, as discussed in the following sections.

The properties of the system with a complex, but commensurate, elementary cell are similar to the properties found above for a simple unit cell with only one atom. Let us consider a rational atomic concentration $\theta = s/q$, where s and q are relatively prime integers, and $s < q$ so that there is no more than one atom in one well of the longitudinal substrate potential. The ground state of the system is still periodic, with period $sa_A = qa_s$, and for V_0 below the bifurcation point, the ground state is again a trivial ground state with $y = 0$ for all atoms. Their x positions along the chain are now shifted from the minima of the potential wells and these shifts increase with V_0, as shown in Fig. 4(a). The elementary cell of the TGS consists now of s atoms. Therefore, the phonon spectrum has to have $2s$ branches, as shown in Fig. 2(b), where for clarity we use the scheme of extended Brillouin zones so that the momentum k varies in the range $|\ k\ | \leq k_\theta$, $k_\theta = sk_B = \theta/2$ with $k_B = \pi/sa_A = 1/2q$ being the boundary of the first Brillouin zone in our units where $a_s = 2\pi$. As shown in Fig. 2(b), the first instability arises again at $k = \pm k_\theta$ and it corresponds to a continuous transition from the TGS to the ZGS. The ZGS has the period $2sa_A$ and a typical ZGS configuration is shown in Fig. 5

for the case $\theta = 5/7$. The qualitative behavior of the model can still be described by Eqs. (19)–(24). For odd s there is one atom at the bottom of a minimum of the substrate potential (i.e., with $\Delta x_i = 0$) due to the symmetry of the model. The displacements Δx_i of the atoms from the bottoms of the substrate potential vary versus V_0, as shown in Fig. 4(a). They have a maximum at the bifurcation point owing to the cusp of the average elastic constant $g(V_0)$, shown in Fig. 4(c), which is similar to the one discussed above for a simpler case. After the bifurcation the longitudinal displacements Δx_i decrease because the average elastic constant is reduced in the zigzag structure with respect to the linear structure. The displacements y in the transverse direction [see Fig. 4(b)] stay on the line $y_i = 0$ before the bifurcation, while after the bifurcation they are split into $2\,\mathrm{Int}[(s+1)/2]$ curves forming two symmetric groups, where Int designates the integer part. The mean displacement b of the atoms in the transverse direction can be estimated from Eq. (20), while the dispersion of the transverse displacements is given approximately by $\Delta b \simeq 2\,|\,(\partial b/\partial a_A)\,|\,\Delta a_A$, where Δa_A is the maximum deviation of interatomic distances along the chain from the average value a_A due to the presence of the substrate potential. Because $\Delta a_A \sim g^{-1}$, we obtain approximately $\Delta b \sim a_A/b\,g$, in agreement with the numerical results of Fig. 4(b).

In addition to the commensurate cases $\theta = 1/q$ and $\theta = s/q$, Figs. 6 and 7 show the numerical results for

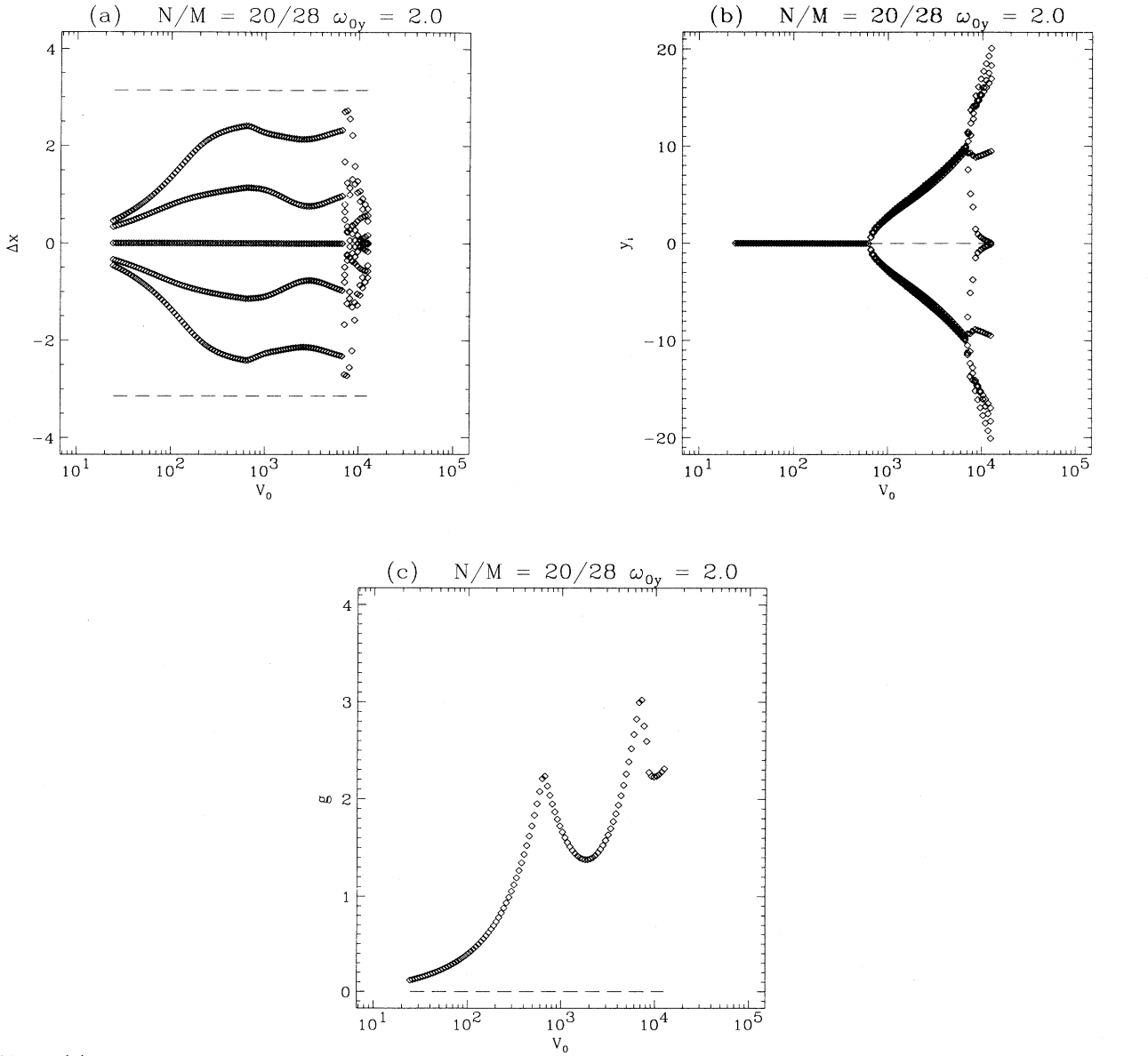

FIG. 4. (a) Longitudinal displacements Δx of the atoms with respect to the nearest minimum of $V_x(x)$ (the dashed horizontal lines indicate the values $\Delta x = \pm\pi$ corresponding to maxima of the substrate potential); (b) transverse displacements; and (c) average elastic constant of the chain as functions of V_0 for $\theta = 5/7$ ($N = 20$, $M = 28$, and $N^* = 60$) and $\omega_{0y} = 2$. The figure shows two bifurcations of the atomic structure.

the cases where the number M of minima of the substrate potential and the number N of atoms are such that $M = N/2 \mp 1$ ($N = 64$ in the calculation). These cases can be interpreted respectively as kink and antikink configurations constructed on the background of the $\theta_0 = 1/2$ GS (more precisely, these configurations correspond to "massive" kinks in terms of [9]). Comparing these results with those for the $\theta = 1/2$ GS of Fig. 3, we see that the critical values of V_0 corresponding to the bifurcation to the ZGS are such that $V_{\rm bif}^{\rm (kink)} < V_{\rm bif}^{\rm (GS)} < V_{\rm bif}^{\rm (antikink)}$, in agreement with Eq. (19), which connects the bifurcation value with the average interatomic distance. For the kink case the TGS-ZGS transition begins in the kink core region, (i.e., in the region of local compression of the chain) and then the zigzag structure extends to the whole system. On the contrary, in the antikink case this transition ends in the antikink core region, which is the region where the chain is stretched locally. In previous works on a generalized FK model similar to this one, some specific properties of the topological excitations for the 2D model with respect to the one-dimensional model have been found [9]. They can be understood in terms of the cusp of the average elastic constant $g(V_0)$. In particular, at $V_0 = V_{\rm bif}^{\rm (GS)}$ the kink core region is already transformed to the zigzag state so that $g_i^{\rm (kink)} < g_i^{\rm (GS)}$. On the other hand, the transition to the zigzag shape within the antikink core region

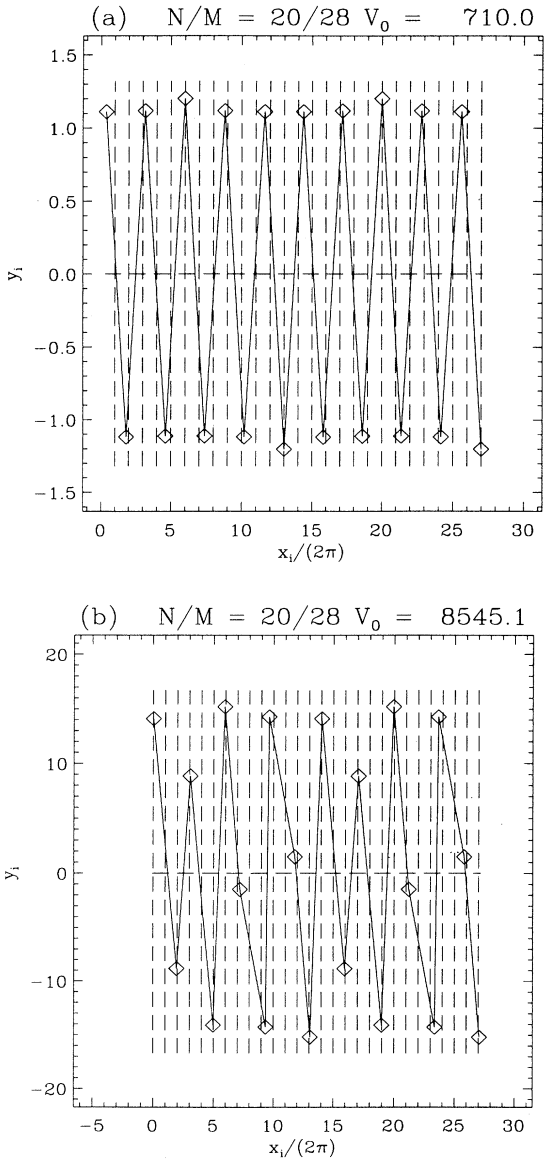

FIG. 5. Typical zigzag GS configuration for $\theta = 5/7$ and $\omega_{0y} = 2$ at (a) $V_0 = 710$, after the first bifurcation, and (b) $V_0 = 8545$, after the second bifurcation.

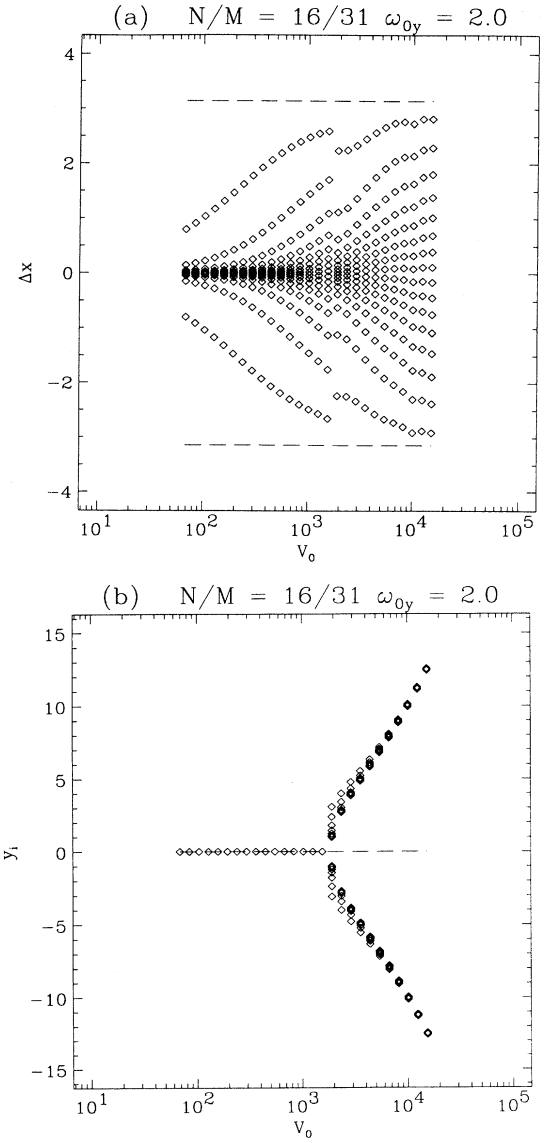

FIG. 6. (a) Longitudinal displacements Δx of the atoms with respect to the nearest minimum of $V_x(x)$ (the dashed horizontal lines indicate the values $\Delta x = \pm\pi$ corresponding to maxima of the substrate potential); (b) transverse displacements y for the configuration of a kink on the background of $\theta_0 = 1/2$ for $\omega_{0y} = 2$ ($\theta = N/M = 16/31$ and $N^* = 64$).

occurs at larger V_0, so that $g_i^{(\text{antikink})} > g_i^{(\text{GS})}$. Because the value of the elastic constant g determines the parameters of the topological excitations such as the effective kink mass m and the height of the Peierls-Nabarro potential ϵ_{PN} (e.g., see [6]), it follows that, at and above the bifurcation, $m^{(\text{kink})} > m^{(\text{antikink})}$ and $\epsilon_{\text{PN}}^{(\text{kink})} > \epsilon_{\text{PN}}^{(\text{antikink})}$. The analysis in terms of effective elastic constant explains the absence of symmetry between a kink and an antikink, which was studied in detail in [9]. Moreover, in the next section we show that the cusp singularity of $g(V_0)$ has also a strong effect on the Aubry transition in the incommensurate case.

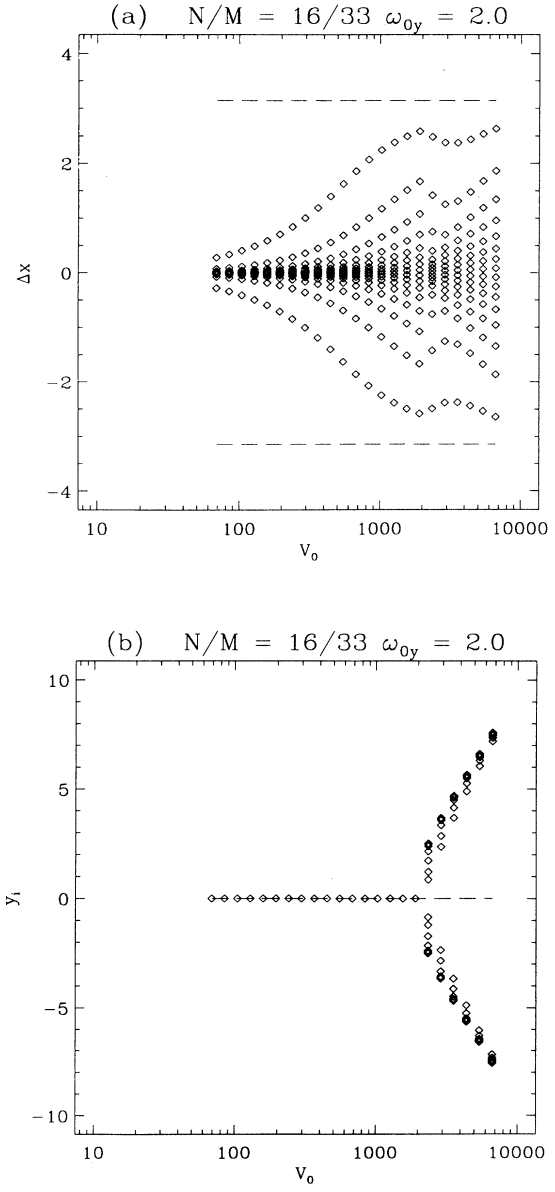

FIG. 7. Same as Fig. 6, but for the antikink configuration ($\theta = N/M = 16/33$).

IV. AUBRY TRANSITIONS

The GS of the standard FK model with an irrational atomic concentration θ corresponds to an incommensurate structure [12,14]. When the elastic constant g_{FK} is increased, this structure exhibits the so-called Aubry transition, which can be understood in terms of the positions of the atoms with respect to the maxima of the substrate potential. For small interactions ($g < g_{\text{Aubry}}$), the on-site potential dominates. The atoms tend to sit near the bottom of the wells and there is a forbidden region near the maxima [Fig. 8(a)]. As a result, the atomic chain is pinned to the substrate because its translation requires moving the atoms up in the substrate potential, over the maxima. On the contrary, for $g > g_{\text{Aubry}}$, the configuration is dominated by the interaction and all the values of the substrate potential are occupied by atoms, some of them being on top of the barrier [Fig. 8(a)]. When the atomic chain is translated over the substrate, some atoms go down in the potential while others go up and there is no barrier to translation. Consequently, below the transition ($g < g_{\text{Aubry}}$) the phonon spectrum has a gap corresponding to the frequency of oscillation of the atomic chain in the pinning potential, while above the transition ($g > g_{\text{Aubry}}$), the gap vanishes. The critical value g_{Aubry} depends on θ; for example, for the "golden mean" concentration $\theta_{\text{gm}} = (1 + \sqrt{5})/2$ the critical elastic constant g_{Aubry} take its maximum value $g_{\text{Aubry}} \sim 1$. The one-dimensional FK model with long-range (but concave) interatomic interactions exhibits qualitatively the same behavior as the standard FK model with nearest-neighbor interactions. The question that arises naturally is to what extent the introduction of a transverse degree of freedom in our model can affect the Aubry transition. The answer can be derived from the variation of the elastic constant g versus V_0 obtained in Sec. III. Because the bifurcation point V_{bif} is determined by the curvature of

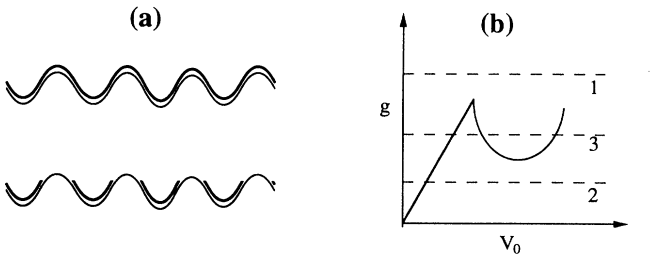

FIG. 8. (a) Schematic diagram of the positions of the atoms with respect to the substrate potential on the two sides of the Aubry transition. The heavy line shows the occupied regions of the potential. For $g < g_{\text{Aubry}}$ (lower figure), the top part of the maxima are not occupied. For $g > g_{\text{Aubry}}$ (top figure), all regions, including the top of the barrier, are occupied. (b) Schematic diagram illustrating the possible competition between the zigzag and the Aubry transitions. The three horizontal lines correspond to the three possible positions of g_{Aubry} with respect to the cusp in the elastic constant due to the transition to a zigzag state: case 1, $g_{\text{Aubry}} > g_{\text{bif}}$; case 2, $g_{\text{Aubry}} < g_{\text{bif}}$ and $g_{\text{Aubry}} < g_{\text{min}}$; case 3, $g_{\text{Aubry}} < g_{\text{bif}}$ and $g_{\text{Aubry}} > g_{\text{min}}$.

the transverse substrate potential $V_{\rm bif} \propto \omega_{0y}^2$ according to Eq. (19) while the Aubry transition concerns essentially the longitudinal displacements, the relative positions of the two transitions can change depending on model parameters. Depending on the value of ω_{0y}^2, we can predict three different scenarios for the behavior of the system with increasing V_0 as shown schematically in Fig. 8(b).

(a) For the case of ω_{0y} below a first threshold ω^*, $\omega_{0y} < \omega^*$, such that $V_{\rm bif} < V_{\rm Aubry}$ (case 1 in Fig. 8), the Aubry transition will not occur because the first bifurcation, to a zig-zag state, which reduces the effective interatomic coupling, occurs before g can reach the magnitude $g_{\rm Aubry}$ required for the Aubry transition, i.e., $g_{\rm bif} < g_{\rm Aubry}$. Taking $g_{\rm Aubry} \simeq 1$ for the golden mean θ_{GM} and $g_{\rm bif} \simeq 9\omega_{0y}^2/16$, the value ω^* can be estimated as $\omega^* \approx 4/3$.

(b) For the case of large ω_{0y}, $\omega_{0y} > \omega^{**}$ (where ω^{**} is a second characteristic value), for which $V_{\rm bif} \gg V_{\rm Aubry}$, $g_{\rm Aubry} < g_{\rm bif}$, and $g_{\rm Aubry} < g_{\rm min} \equiv \min g(V_0)$ for all V_0 within the ZGS (case 2 in Fig. 8), the Aubry transition is observed when V_0 reaches $V_{\rm Aubry}$ and the bifurcation that occurs later does not bring any qualitative change in the system behavior because the minimum of g after the bifurcation is above $g_{\rm Aubry}$. Only a higher-order bifurcation (see Sec. V) could bring a qualitative change. Taking $g_{\rm min} \simeq 0.5 g_{\rm bif}$, the value ω^{**} can be estimated as $\omega^{**} \approx 4\sqrt{2}/3 \approx 1.9$ for $\theta = \theta_{\rm GM}$.

(c) For intermediate ω_{0y}, $\omega^* < \omega_{0y} < \omega^{**}$ (case 3 in Fig. 8), such that $g_{\rm Aubry} < g_{\rm bif}$ but $g_{\rm Aubry} > g_{\rm min}$, when V_0 is increased, the system undergoes first an Aubry transition in which the pinned GS is transformed to a sliding GS. But then the bifurcation to a zigzag state can reduce the average elastic constant below $g_{\rm Aubry}$. The system undergoes a *reverse* Aubry transition and the lattice gets pinned to the substrate again. The further increase of g that occurs after the minimum can cause again a direct Aubry transition restoring the sliding state, at least up to the second bifurcation.

In order to check numerically these predictions, we should in principle choose N/M irrational, which is not possible for a finite system because M and N must be integers in our calculations. There are, however, sequences of rational numbers that approach closely an irrational number. They can be obtained from the continuous fraction expansion of the irrational number. An example is provided by the Fibbonacci sequence

$$1 \to \frac{2}{3} \to \frac{3}{4} \to \frac{5}{7} \to \frac{8}{11} \to \frac{13}{18} \to \frac{21}{29} \to \frac{34}{47} \to \cdots, \quad (25)$$

which tends to $\theta'_{GM} = (3+\sqrt{5})/(5+\sqrt{5})$, equivalent to the golden mean for the Aubry transition. We chose $N = 34$, $M = 47$, and $N^* = 34$ in our study. The results of the numerical calculations are presented in Figs. 9–11. Let us consider first the case of the transverse frequency $\omega_{0y} = 1$ (Fig. 9), which is expected to correspond to case (a). In this case, for the trivial GS, the elastic constant g increases with V_0 and reaches the maximum $g_{\rm bif} = 0.533$ at $V_{\rm bif} = 137$. After the TGS-ZGS transition, g begins to decrease, reaches the minimum $g_{\rm min} = 0.330$ at $V_0 = 397$, and then rises again to reach $g_{\rm bif}^{(2)} = 0.734$ at $V_{\rm bif}^{(2)} = 1569$, where the second bifurcation takes place. However, for all values of V_0 the elastic constant does not reach the threshold value $g_{\rm Aubry} \simeq 1$ and the Aubry transition cannot occur. Indeed, Fig. 9(a) shows that longitudinal atomic displacements from the bottoms of the wells are always smaller that $a_s/2 = \pi$. This corresponds to the case below the Aubry transition for which longitudinal displacements that bring the atoms near the maxima of the potential are forbidden. Therefore, for this case the GS is pinned for all V_0.

Second, we take $\omega_{0y} = 2$ in order to simulate case (b). For this transverse frequency we obtain $g_{\rm bif} = 2.274$ at

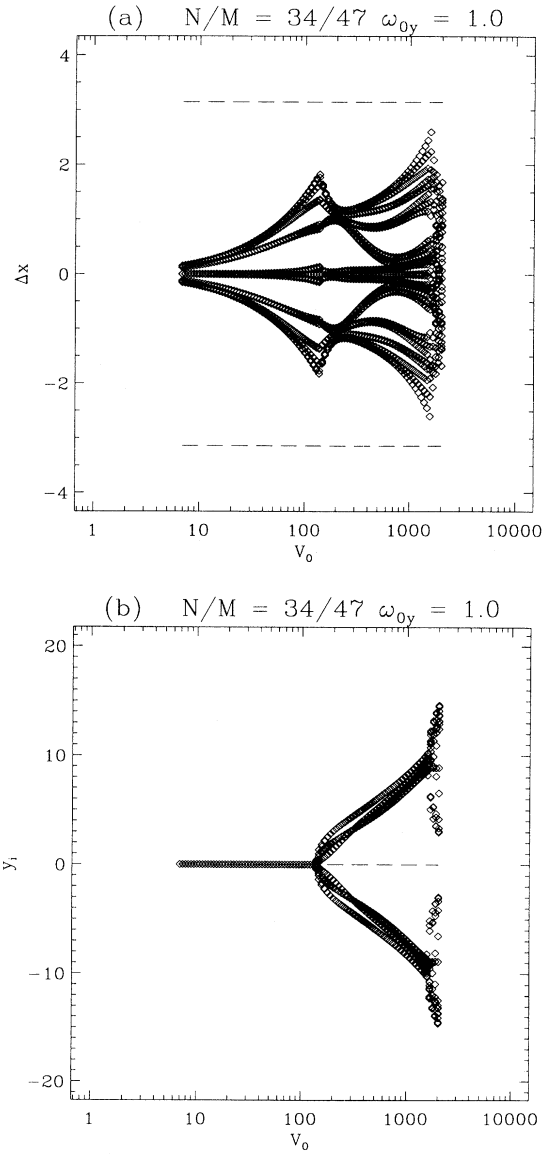

FIG. 9. (a) Longitudinal displacements Δx of the atoms with respect to the nearest minimum of $V_x(x)$ (the dashed horizontal lines indicate the values $\Delta x = \pm\pi$ corresponding to maxima of the substrate potential); (b) transverse displacements y versus V_0 for the incommensurate structure ($\theta = 34/47$ and $N^* = 34$) for $\omega_{0y} = 1$.

$V_{\rm bif} = 624$, $g_{\rm min} = 1.379$ at $V_0 = 1802$, and $g_{\rm bif}^{(2)} = 3.09$ ($V_{\rm bif}^{(2)} = 6681$). Now $g_{\rm bif} \gg g_{\rm Aubry}$ and the Aubry transition is expected to occur before the bifurcation to a zigzag state. Moreover, the sliding state can survive up to the second bifurcation because $g_{\rm min} > g_{\rm Aubry}$. Indeed, the numerical results of Fig. 10(a) show that the Aubry transition takes place at $V_{\rm Aubry} = 260$ when for the first time at least one atom reaches the longitudinal displacement $\Delta x_i \simeq \pi$. Remember that the presence of an atom on a maximum of the substrate potential $V_x(x)$ usually indicates that this state is free to slide on the substrate. The average elastic constant determined numerically is $g_{\rm Aubry} \approx 1$, as expected. After the bifurcation the atomic displacements decrease slightly; however, up to the second bifurcation, the figure still shows atoms close to potential maxima. One should notice that, because we perform the calculation with a finite number of atoms, the value corresponding *exactly* to the potential maximum may not always be occupied in our results, even if we have a sliding phase. The results suggest, however, that the sliding phase persists up to the second bifurcation point. A more sensitive test is provided by the calculation of the linear response of the atomic chain to an external force F applied to all the atoms, along the direction of the x axis. We calculate the mean shift of the atoms $\Delta x_{\rm shift} = (1/N)\sum_{i=1}^{N}(x_i - x_i^{(0)})$ with respect to their positions without the force $x_i^{(0)}$ and define a susceptibility as

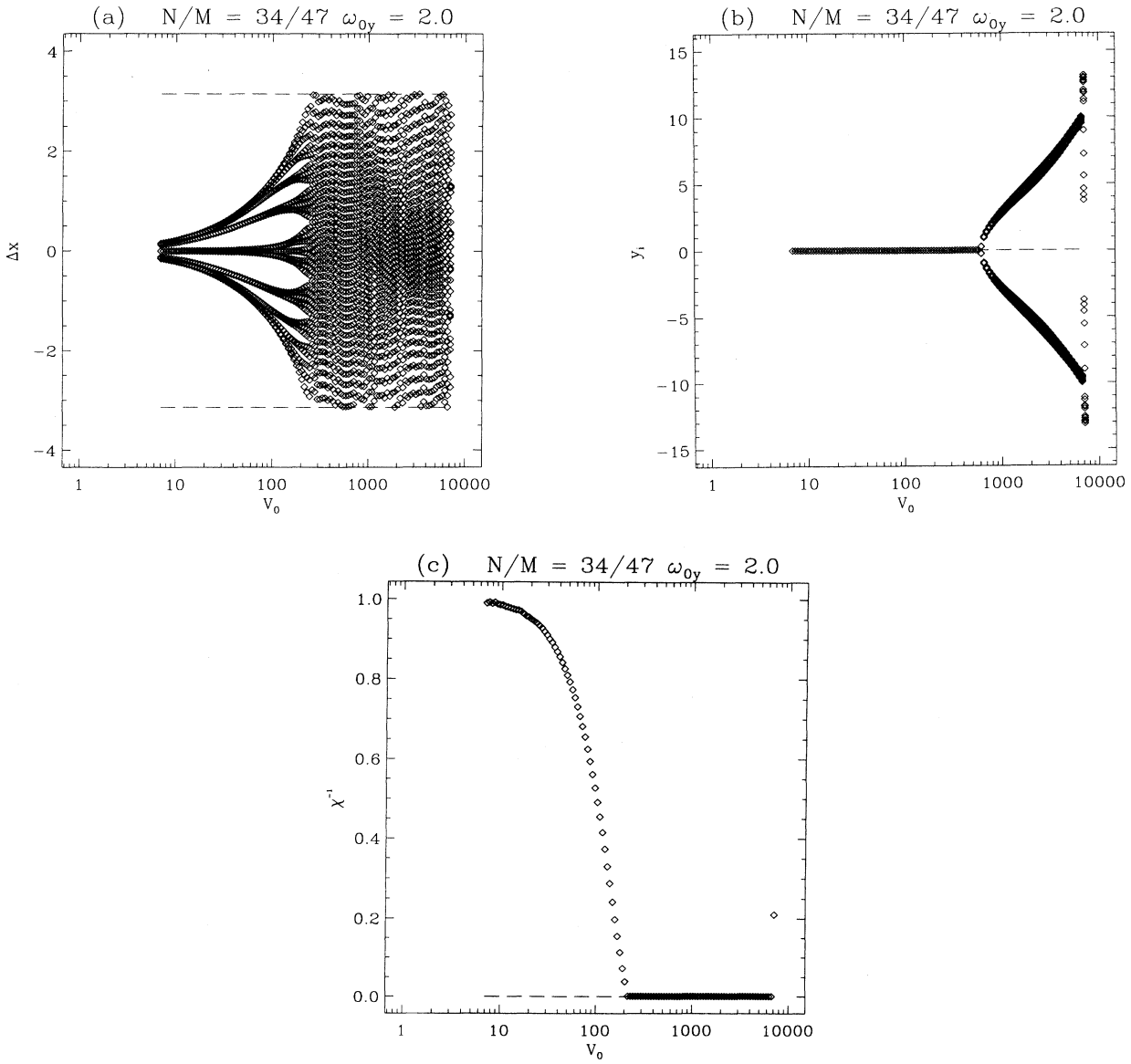

FIG. 10. (a) Longitudinal displacements Δx of the atoms with respect to the nearest minimum of $V_x(x)$ (the dashed horizontal lines indicate the values $\Delta x = \pm\pi$ corresponding to maxima of the substrate potential); (b) transverse displacements y; and (c) inverse susceptibility χ^{-1} versus V_0 for the incommensurate structure ($\theta = 34/47$ and $N^* = 34$) for $\omega_{0y} = 2$.

$$\chi = \Delta x_{\rm shift}/F. \tag{26}$$

We expect $\chi \to \omega_{0x}^{-2}$ in the limit $V_0 \to 0$ and $\chi \to \infty$ in the sliding state. Note, however, that in a numerical simulation the value θ is always rational, so the GS will stay slightly pinned. The results of the simulation [see Fig. 10(c) where we took $F = 0.001$] show a sharp drop of χ^{-1} when the Aubry transition is reached and then χ^{-1} stays practically equal to zero ($\chi^{-1} \approx 0.0005$) for the whole range $V_{\rm Aubry} < V_0 < V_{\rm bif}^{(2)}$, so that the GS in this case is really very close to the sliding state in spite of the finiteness of our system.

Last, to simulate the intermediate case (c), we take $\omega_{0y} = 1.5$. The results are presented in Fig. 11. As in the previous case, the Aubry transition that occurs at $V_0 = 231$ ($g = 0.86$) takes place before the bifurcation and then g continues to rise to the value $g_{\rm bif} = 1.268$ [see Fig. 11(b)]. But after the bifurcation that takes place at $V_{\rm bif} = 381$, the elastic constant g decreases and reaches the minimum $g_{\rm min} = 0.766$, which is lower than $g_{\rm Aubry}$ at $V_0 = 993$. Figure 11 shows that, in the vicinity of the minimum of the function $g(V_0)$, the atomic displacements decrease strongly and there is no longer an atom on top of the maxima of $V_x(x)$. Thus, in the region near the minimum of $g(V_0)$, the GS again seems pinned. This is confirmed by the behavior of the susceptibility [Fig. 11(c)], which attests that we have observed the predicted reverse Aubry transition from the sliding to the pinned state at $V_0 = 414$ when $g = 1.11$. With a further increase of V_0, after reaching the minimum the

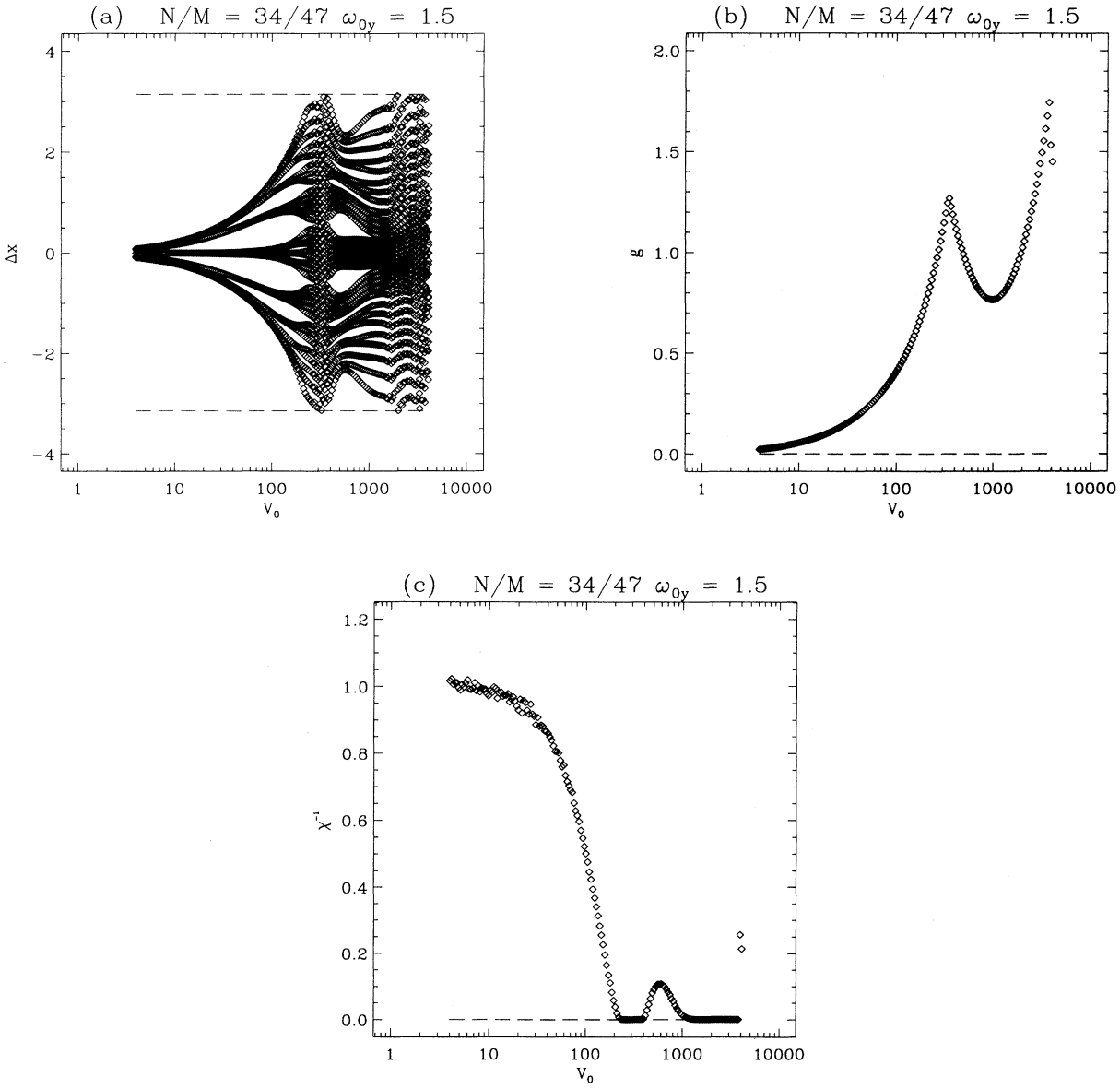

FIG. 11. Same as Fig. 10, but for $\omega_{0y} = 1.5$. The inverse susceptibility shows the existence of a reverse Aubry transition followed again by a direct transition for which χ^{-1} drops again to 0.

elastic constant increases again and at $V_0 = 1445$ when $g = 0.840$ the system undergoes a second direct Aubry transition before the second bifurcation. The two transitions from the pinned to the sliding state (direct Aubry transitions) have been found in our calculations for an average elastic constant $g \simeq 0.85$, while the transition from the sliding to the pinned state (reverse Aubry transition) is obtained for $g = 1.11$. Although these values are close to the expected value $g \simeq 1$, they suggest a small hysteresis effect at the transition. However, it could be due to the finiteness of the system (M/N is not truly irrational) or to the limited accuracy of our susceptibility measurements [in order to determine the susceptibility of Fig. 11(c) we have measured the response of the system to a force $F = 0.0001$; although it is very small, in the immediate vicinity of the transition the system may not be in the linear response regime].

V. HIGHER-ORDER BIFURCATIONS

As mentioned in the Introduction, taking into account long-range forces and not only nearest-neighbor interactions allows further bifurcations beyond the first instability leading to the ZGS. Figure 4 shows, for instance, the existence of a second bifurcation at $V_0 = 7111$ for $\theta = 5/7$. This bifurcation induces a second cusp in the elastic constant, as shown in Fig. 4(c), and leads to the atomic configuration shown in Fig. 5. Figure 10 shows another example of a second bifurcation observed in an "incommensurate" case $\theta = 34/47$. Contrary to the case shown in Fig. 4, this bifurcation is a first-order (discontinuous) transition that leads to an abrupt drop in the average elastic constant. To investigate the stability of the zigzag configuration and detect the possible existence of other bifurcations, we must calculate its phonon spectrum. In order to obtain analytical estimates we restrict ourselves to the simplest case of $\theta = 1$ and the interaction of nearest and next nearest neighbors only. Substituting the atomic coordinates $x_i^{(0)} = ia_s$ and $y_i^{(0)} = (-1)^i b$ into Eq. (7a), we obtain for the elastic matrix $\mathbf{A}$ the expressions

$$A_{11}^{xx} = \omega_{0x}^2 + 2V_0 d^{-5}\left[2a_s^2 - 4b^2\right] + \frac{1}{2}V_0 a_s^{-3}, \tag{27}$$

$$A_{11}^{yy} = \omega_{0y}^2 + 2V_0 d^{-5}\left[8b^2 - a_s^2\right] - \frac{1}{4}V_0 a_s^{-3},$$

$$A_{11}^{xy} = 0,$$

$$A_{12}^{xx} = -V_0 d^{-5}\left[2a_s^2 - 4b^2\right],$$

$$A_{12}^{yy} = -V_0 d^{-5}\left[8b^2 - a_s^2\right],$$

$$A_{12}^{xy} = -A_{10}^{xy} = -6V_0 d^{-5} a_s b,$$

$$A_{13}^{xx} = -\frac{1}{4}V_0 a_s^{-3},$$

$$A_{13}^{yy} = \frac{1}{8}V_0 a_s^{-3},$$

$$A_{13}^{xy} = 0.$$

Its Fourier transform (8) is

$$D_{11}^{xx}(k) = \omega_{0x}^2 + \frac{1}{2}\omega_{0y}^2\frac{3-v^2}{v^2} + \frac{1}{8}\omega_{0y}^2 v^3[1-\cos(2ka_s)], \tag{28}$$

$$D_{11}^{yy}(k) = \omega_{0y}^2 + \frac{1}{2}\omega_{0y}^2\frac{2v^2-3}{v^2} - \frac{1}{16}\omega_{0y}^2 v^3[1-\cos(2ka_s)],$$

$$D_{12}^{xx}(k) = -\frac{1}{4}\omega_{0y}^2\frac{3-v^2}{v^2}(1+e^{-i2ka_s}),$$

$$D_{12}^{yy}(k) = -\frac{1}{4}\omega_{0y}^2\frac{2v^2-3}{v^2}(1+e^{-i2ka_s}),$$

$$D_{12}^{xy}(k) = -\left[D_{21}^{xy}(k)\right]^* = -\frac{3}{4}\omega_{0y}^2\frac{\sqrt{v^2-1}}{v^2}(1+e^{-i2ka_s}),$$

where $|k| \leq \frac{1}{4}$ and we have used the dimensionless variable v instead of V_0 according to Eq. (22).

The phonon spectrum is determined by the roots of Eq. (9), which now takes the form

$$(\omega^2-\alpha-\gamma)(\omega^2-\alpha+\gamma)(\omega^2-\beta-\delta)(\omega^2-\beta+\delta)$$

$$-2\epsilon^2[(\omega^2-\alpha)(\omega^2-\beta)+\gamma\delta]+\epsilon^4 = 0, \tag{29}$$

where $\alpha = D_{11}^{xx}(k)$ $\beta = D_{11}^{yy}(k)$, $\gamma = |D_{12}^{xx}(k)|$, $\delta = |D_{12}^{yy}(k)|$, and $\epsilon = |D_{12}^{xy}(k)|$ depend on k. Because the zigzag configuration for $\theta = 1$ has two atoms in the elementary cell, the phonon spectrum consists of four branches $\omega_j(k)$, j=1–4. Contrary to the case of the TGS, in the ZGS x and y modes are coupled. In order to find an instability point $v_{\rm crit}$, we have to take the lowest root $\omega_{\min}(k) = \min_j \omega_j(k)$ of Eq. (29) and then look for the point where $\omega_{\min}(k)$ reaches zero for the first time at some $k = k^*$.

An investigation of Eq. (29) shows that the value k^* depends on the ratio $\Omega_y = \omega_{0y}/\omega_{0x}$. Namely, at high Ω_y, $\Omega_y > \Omega_{\rm crit}$ (the critical value $\Omega_{\rm crit}$ is about 1.52; note that $\Omega_{\rm crit} > 1$), the instability occurs for momentum $k^* = 0$. But for $k = 0$ we have $\epsilon = 0$ in Eq. (29) so that the motions along the x and the y directions are decoupled and their eigenfrequencies are equal $\omega_1^2(0) = \omega_{0x}^2 + \omega_{0y}^2(3-v^2)/v^2$, $\omega_2^2(0) = \omega_{0x}^2$, $\omega_3^2(0) = \omega_{0y}^2 + \omega_{0y}^2(2v^2-3)/v^2$, and $\omega_4^2(0) = \omega_{0y}^2$. Thus $\omega_1(0)$ corresponds to the lowest frequency and it becomes equal to zero at the critical amplitude of repulsion

$$v_{\rm crit} = \sqrt{3}\omega_{0y}/\sqrt{\omega_{0y}^2 - \omega_{0x}^2}. \tag{30}$$

The mode $\omega_1(0)$ corresponds to motion of the upper and the lower subchains of the zigzag configuration in opposite directions along the chain.

On the other hand, at low transverse frequency, $\Omega_y < \Omega_{\rm crit}$, the instability condition $\omega_{\min}(k^*) = 0$ is satisfied for the first time at a nonzero momentum k^*, where the value k^* is close to the Brillouin zone boundary

$k_B = \frac{1}{4}$. In particular, near the critical point we find that $k^* = 0.852k_B$ for $\Omega_y = 1.5$ and the corresponding critical repulsion is $v_{\rm crit} = 2.305$. For lower values of ω_{0y} the critical momentum k^* and the repulsion amplitude $v_{\rm crit}$ increase slightly. For example, we find that $k^* = 0.854k_B$ and $v_{\rm crit} = 2.315$ for $\Omega_y = 1$, $k^* = 0.858k_B$ and $v_{\rm crit} = 2.337$ for $\Omega_y = 0.5$, and $k^* = 0.858k_B$ and $v_{\rm crit} = 2.364$ in the limit $\Omega_y \to 0$. Because k^* is now close to k_B, the zigzag configuration is unstable with respect to creation of an incommensurate configuration, which is close to the subzigzag configuration where the atoms in both (upper and lower) subchains are predominantly shifted in opposite y directions.

However, before the critical point $v_{\rm crit}$ where the zigzag configuration becomes unstable, it becomes metastable at a point $v_{\rm bif}^{(2)}$. The rhomboid configuration of Fig. 1(c) which was metastable for $v < v_{\rm bif}^{(2)}$, becomes the minimum-energy configuration above the second bifurcation point. The rhomboid configuration remains the GS configuration up to the next bifurcation $v_{\rm bif}^{(3)}$, when it is substituted by the double zigzag configuration of Fig. 1(d), then at $v = v_{\rm bif}^{(4)}$ by the hexagonal configuration of Fig. 1(e), and so on. Thus, beginning from the ZGS, the ground state of the system undergoes a series of first-order transitions with increasing interatomic repulsion.

When the longitudinal substrate potential is negligible (e.g., when $\omega_{0y} \gg \omega_{0x}$), the sequence of the ground-state configurations may be viewed as broader and broader stripes cut out from the 2D hexagonal lattice (see Fig. 1), where the longitudinal lattice constant $a_{\rm cell}$ is determined by the atomic concentration θ [$a_{\rm cell} = (a_s/\theta)s'$, $s' = 2, 3, 4, 5, \ldots$ for the zigzag, rhomboid, double zigzag, hexagonal, etc., configurations, respectively], while the transverse atomic displacements evolve to adjust to the transverse potential $V_y(y)$. When the amplitude of the longitudinal potential $V_x(x)$ increases, the atoms tend to move to the nearest minima of $V_x(x)$. Therefore the positions of the bifurcation points $V_{\rm bif}^{(m)}$ should depend on ω_{0y} as well as on the atomic concentration $\theta = s/q$, because a configuration is expected to be more stable when the integers s and s' match (for example, see the rhomboid configuration for $\theta = 3/4$ in Fig. 12).

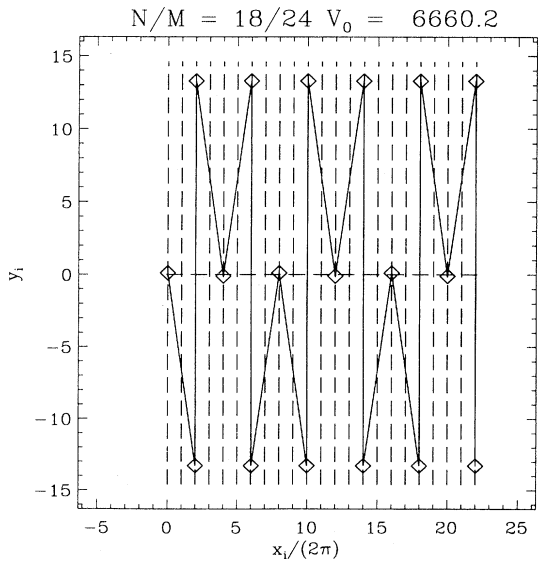

FIG. 12. Rhomboid configuration for $\theta = 3/4$ ($N = 18$, $M = 24$, and $N^* = 36$) and $\omega_{0y} = 2$ at $V_0 = 6660$.

These predictions are based on analytical expressions in the case $\theta = 1$ with only nearest and next nearest interactions. They should be checked by numerical calculations as done in the previous sections. However, the calculations become very difficult because, for complicated structures, it is very difficult to make sure that we have obtained the true ground state after relaxation. Therefore we have limited our investigations to a few particular situations such as the one shown in Fig. 12 or the second bifurcations shown in Figs. 4 and 10 without attempting an exhaustive study, which would have been of limited physical interest because the perfectly symmetric potential is an idealized case. As discussed in the next section, as soon as some asymmetry is introduced, the picture changes qualitatively.

VI. ASYMMETRIC MODEL

In many physical systems such as adsorbed films, the external potential in the transverse direction is not symmetric. Let us discuss a possible modification of the behavior of the system when $V_y(y)$ is asymmetric. As an example we take an anharmonic Toda-like potential

$$V_y(y) = \omega_{0y}^2 y_{\rm anh}^2 \left[\exp(-y/y_{\rm anh}) + (y/y_{\rm anh}) - 1\right], \quad (31)$$

where $\beta = y_{\rm anh}^{-1}$ is the anharmonic constant; in the limit $\beta \to 0$ this function reduces to the harmonic form (3) studied above. Numerical calculations show that the behavior of the system before the second bifurcation $V_0 < V_{\rm bif}^{(2)}$ is practically the same as for the symmetric model. The only differences are that now the zigzag GS is asymmetric and the y displacements for the upper subchain ($y > 0$) $b_{\rm up}$ are larger than those for the lower subchain ($y < 0$) $b_{\rm down}$. As a result, the figure showing the bifurcation in y is asymmetric, as shown in Fig. 13(a). Above the second bifurcation, however, the scenario is different from that of the symmetric model.

We can analyze the zigzag configuration as a system of two subchains. Let us neglect temporarily the interaction between the subchains. In analogy with the mechanism of the first bifurcation, if V_0 increases, the atoms in a given subchain tend to increase their interatomic distances and at a certain threshold value of V_0 the subchain may evolve into a zigzag shape as the original chain does for the first bifurcation. In the symmetric model such a mechanism of the second bifurcation is ineffective because the instabilities of both (upper and lower) subchains occur simultaneously. At this point, even a very small interaction between the subchains destroys this scenario. This is why we had to treat the two subchains simultaneously, leading to the fourth order Eq. (29) for ω^2. For an asymmetric model, however, the instabilities in the upper and the lower subchains occur sequentially.

The bifurcation points are determined by the curvature of $V_y(y)$ for y equal to atomic coordinates in one subchain. To find the bifurcation points, we can deduce, similarly to Eq. (19), an equation

$$V_{\rm bif}^{(m)} = \frac{1}{4}(\omega_{\rm eff}^{(m)})^2(2^{m-1}a_A)^3 , \qquad (32)$$

where we have introduced $\omega_{\rm eff}^2 = \left[\frac{\partial^2}{\partial y^2}V_{\rm sub}(r)\right]_{r=r_i}$ instead of ω_{0y}^2. Because $\omega_{\rm eff}^2 = \omega_{0y}^2\exp(-\beta y)$ for the Toda potential (31), we see that the upper and the lower subchains are now characterized by different effective frequencies $\omega_{\rm eff}^{\rm up}$ and $\omega_{\rm eff}^{\rm down}$ such that $\omega_{\rm eff}^{\rm up} < \omega_{0y} < \omega_{\rm eff}^{\rm down}$. So the instability arises first at $V_0 = V_{\rm bif}^{(\rm up)}$ in the upper subchain and leads to creation of a subzigzag GS configuration in the upper subchain only [Fig. 13(c)]. Then, at $V_0 = V_{\rm bif}^{(\rm down)} > V_{\rm bif}^{(\rm up)}$, the lower subchain becomes unstable, creating a subzigzag configuration in the lower subchain too [Fig. 13(d)]. Thus the second bifurcation leads to splitting of the two-subchain structure into a three-subchain configuration, then into a four-subchain configuration. As we consider an interaction between all the atoms of the system, when a subchain is created, the atoms belonging to this chain do interact with each other. This is why we can treat it, at least approximately, as we have done for the chain of the TGS. We could thus expect that the evolution of the GS configuration would proceed in an analogous manner: additional bifurcations could start on the top subchain leading to the creation

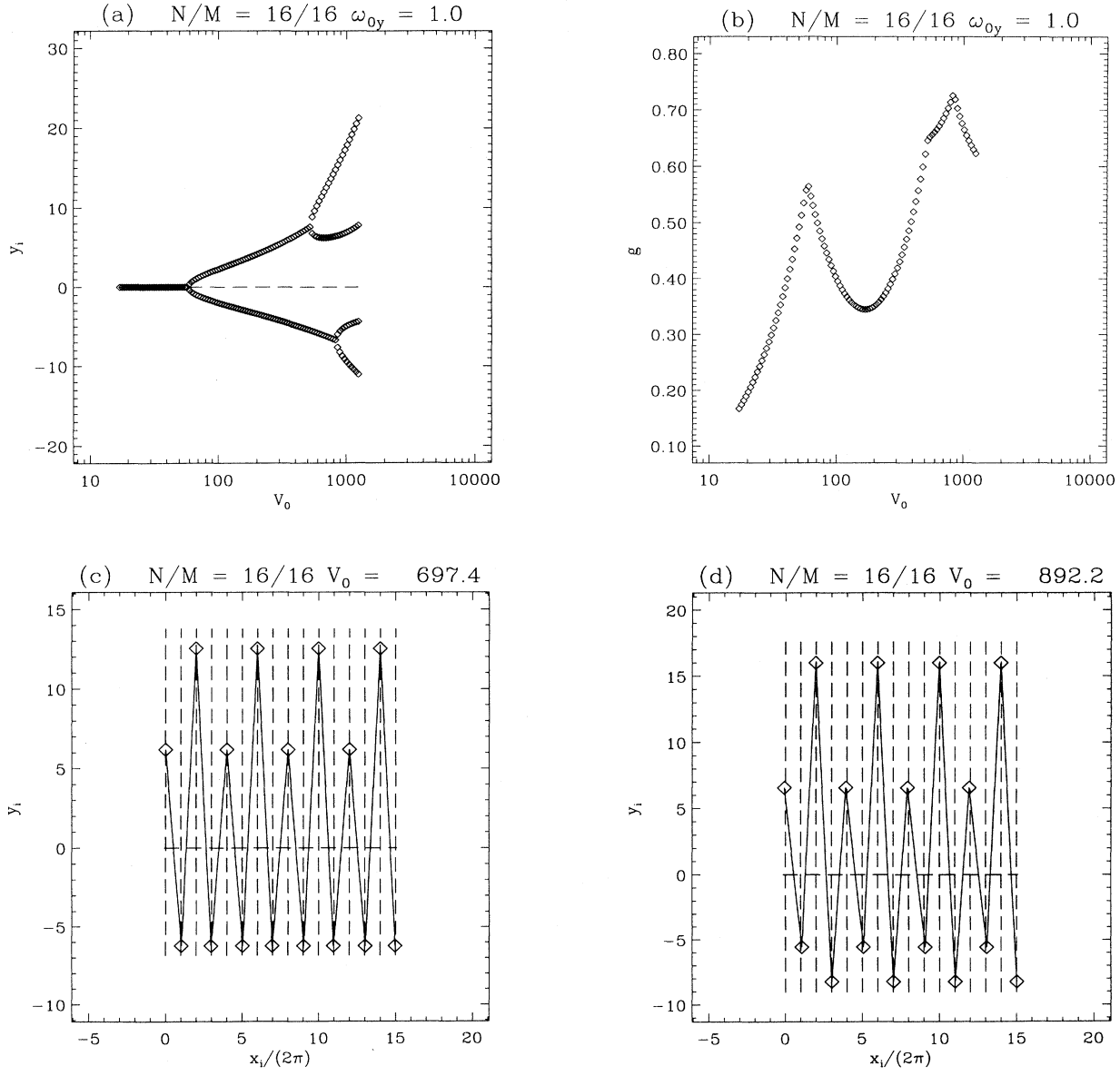

FIG. 13. (a) Transverse atomic displacements; (b) elastic constant g versus V_0; and two typical configurations for (c) $V_0 = 697$ and (d) $V_0 = 892$ for the Toda transverse substrate potential. $\theta = 1$ ($N = M = 16$ and $N^* = 64$), $\omega_{0y} = 1$, and $y_{\rm anh} = 20$.

of the next subzigzag structure (i.e., the next splitting of the top subchain) and then this splitting would spread sequentially to subchains with smaller y values. This scenario reminds one of the well-known Feigenbaum picture for the transition from a regular to the chaotic behavior, so it should end at some accumulation point by the of an incommensurate structure for a rational θ (as for the Aubry transition, the resulting configuration did not need to be a chaotic configuration, but a regular configuration belonging to the Cantor set embedded into a chaotic set of configurations). In our model, however, the accumulation point lies at infinity according to Eq. (32).

Thus, in the asymmetric model, not only the first bifurcation, but also a few additional bifurcations correspond to second-order transitions. The picture discussed above is, however, oversimplified because the distance between the central subchains (i.e., the subchains with the smallest transverse displacements) does not increase fast enough and the interaction between them increases with V_0. Therefore they cannot be treated as independent and the coupling, which generates a first-order transition in the symmetric case, could well do the same for the asymmetric transverse potential. The high-order bifurcations predicted by this discussion are very difficult to observe numerically and, as shown in Fig. 13, we have seen only three bifurcations (leading to the splitting of the system into four subchains) in our calculations.

VII. DISCUSSION

In the present paper we have investigated a generalized FK model with a transverse degree of freedom for an arbitrary atomic concentration θ. We have shown that with increasing interatomic repulsion the trivial GS of the system, where all atoms are aligned on the line $y = 0$, undergoes a series of bifurcations producing first a zigzag GS and then configurations with a more complicated structure. The bifurcations generate cusps in the variation of the elastic constant g versus the magnitude of the interatomic interaction V_0. These singularities of $g(V_0)$ result in significant modifications of the properties of the system and in particular they change the scenario of the Aubry transition for incommensurate phases.

Let us try to determine whether the bifurcations could take place in a real physical systems such as atoms in the channel of a superionic conductors or protons in hydrogen-bonded chains (for instance, in the ion channels of biomembranes). To estimate the value of the transverse frequency ω_{0y}, we may assume that, in a crystal, $V_y(y)$ results also from a periodic potential $V_y(y) = \frac{1}{2}\epsilon_{sy}[1 - \cos(2\pi y/a_{sy})]$, where ϵ_{sy} is the characteristic amplitude and a_{sy} is the characteristic distance for the transverse potential. For this shape of $V_y(y)$ we obtain $\omega_{0y}^2 = V_y''(0) = 2\pi^2\epsilon_{sy}/a_{sy}^2$. For ions with a unit elementary charge e, $V_0 = e^2$ in Eq. (4). Then, setting $a_A = a_s/\theta$, in Eq. (19), we find that the TGS-ZGS bifurcation takes place when θ reaches a threshold value

$$\theta_{\rm bif} = \left[\frac{\pi^2}{2}\left(\frac{a_s}{a_{sy}}\right)^2 \frac{\epsilon_{sy}}{e^2/a_s}\right]^{1/3}. \tag{33}$$

Taking $a_s \sim a_{sy} \sim 3$ Å and $\epsilon_{sy} \sim 0.1$ eV, we obtain $\theta_{\rm bif} \sim 0.5$. This is a value that can easily be achieved in a real system. Thus it seems likely that the usual picture of ions staying in line in a channel is oversimplified. According to our results, the possibility of ionic motion in transverse directions could modify significantly some conclusions obtained earlier within the framework of the standard FK model.

It is clear that accounting for transverse degrees of freedom is very important in modeling the adsorbed layers as well as in studies of the crowdion problem. In particular, the TGS-ZGS transition occurring with an increase of the atomic concentration drastically decreases the mobility of topological excitations in this systems [9]. To study these effects numerically we should, however, use a more realistic model with, e.g., a Morse-type interatomic potential. Moreover, in adsorbed systems the transverse potential is nonconvex, so the realistic model should use the Morse potential for the $V_y(y)$ too. A sequence of the GS configurations with θ increasing for a model generalized in this way can simulate crystal growth process [17].

In the present work we restricted ourselves to investigation of the ground-state configurations only. However, another aspect of the model is that it has a large number of metastable states for all values of V_0, contrary to the standard FK model, where the number of metastable states goes to zero with increasing V_0 [15]. To investigate the metastable configurations, we first have to study topological excitations, i.e., to determine the characteristics of kinklike excitations. Note that the more complicated the structure of the GS, the larger the number of different types of kinks. For example, the TGS admits two kink configurations only (kinks and antikinks), while the ZGS admits already four types of kinks ("massive" and "nonmassive" kinks and antikinks; see [9]). The knowledge of kink parameters is necessary for developing the phenomenological theory of low-temperature system dynamics. For example, in the one-dimensional FK model the phenomenological theory [16] predicts an irregular shape for the dependence of the system conductivity on atomic concentration and a devil's staircase shape for the same dependence of the chemical diffusion coefficient. The investigation of a modification of these dependences in a more realistic model with a transverse degree of freedom would have a great interest. The first step in this direction has been done in [9], where kink parameters were found for the simplest case of $\theta = 1$.

Of course, the model with a single atomic chain is oversimplified; real physical objects have to be modeled by a system of parallel chains [7]. So the generalization of the model with transverse degrees of freedom in this way is very desirable too. Such an investigation would be one step toward the understanding of the vector 2D FK model.

Finally, in this work we have discussed only the static properties of the model. The dynamics of a model with a transverse degree of freedom is certainly very different from the dynamics of the standard FK model even for the TGS. For example, it is possible that statically unstable configurations become dynamically stable. An investigation of these questions would also be interesting.

ACKNOWLEDGMENTS

This work was supported in part by the NATO Linkage Grant No. LG 930236. One of us (O.M.B.) was partially supported by a Soros grant awarded by the American Physical Society. The main part of this work was done during a stay of O.M.B. at the Ecole Normale Supérieure de Lyon and was completed during a visit of M.P. at the Institute of Physics of Kiev. Both authors want to acknowledge the warm hospitality at these institutions.

[1] J.B. Boyce and B.A. Huberman, Phys. Rep. **51**, 189 (1979).

[2] Ya.I. Frenkel, *Introduction into the Theory of Metals* (Nauka, Leningrad, 1972).

[3] I.F. Lyuksyutov, A.G. Naumovets, and V.L. Pokrovsky, *Two-Dimensional Crystals* (Naukova Dumka, Kiev, 1988 and Academic Press, Boston, 1992).

[4] A.S. Davydov, *Solitons in Molecular Systems* (Naukova Dumka, Kiev, 1984 and Reidel Publishing, Dordrecht, 1983).

[5] Ya. Frenkel and T. Kontorova, Phys. Z. Sowietunion **13**, 1 (1938); Zh. Eksp. Teor. Fiz. **8**, 89 (1938); J. Phys. (Moscow) **1**, 137 (1939).

[6] O.M. Braun and Yu.S. Kivshar, Phys. Rep. (to be published).

[7] F. Yoshida, Y. Okwamoto, and T. Nakayama, J. Phys. Soc. Jpn. **50**, 1039 (1981); **51**, 1329 (1982); H. Kato, Y. Okwamoto, and T. Nakayama, *ibid.* **52**, 3334 (1983); J. Pouget, S. Aubry, A.R. Bishop, and P.S. Lomdahl, Phys. Rev. B **39**, 9500 (1989); O.M. Braun, Yu.S. Kivshar, and A.M. Kosevich, J. Phys. C **21**, 3881 (1988); O.M. Braun and Yu.S. Kivshar, J. Phys. Condens. Matter **2**, 5961 (1990); see also Ref. [3].

[8] J.H. van der Merwe, J. Appl. Phys. **41**, 4725 (1970); J.A. Snyman and J.H. van der Merwe, Surf. Sci. **45**, 619 (1974); J.A. Snyman and H.C. Snyman, *ibid.* **105**, 357 (1981); F.F. Abraham, W.E. Rudge, D. Auerbach, and S.W. Koch, Phys. Rev. Lett. **52**, 445 (1984); P.S. Lomdahl and D.J. Srolovitz, *ibid.* **57**, 2702 (1986); D.J. Srolovitz and P.S. Lomdahl, Physica D **23**, 402 (1986); W. Uhler and R. Schilling, Phys. Rev. B **37**, 5787 (1988).

[9] O.M. Braun and Yu.S. Kivshar, Phys. Rev. B **44**, 7694 (1991); O.M. Braun, O.A. Chubykalo, Yu.S. Kivshar, and L. Vázquez, *ibid.* **48**, 3734 (1993).

[10] O.M. Braun and V.K. Medvedev, Usp. Fiz. Nauk **157**, 631 (1989) [Sov. Phys. Usp. **32**, 328 (1989)].

[11] A.A. Maradudin, *Theoretical and Experimental Aspects of the Effects of Point Defects and Disorder on the Vibrations of Crystals* (Academic, New York, 1966); A.M. Kosevich, *Fundamentals of Crystal Lattice Mechanics* (Nauka, Moscow, 1972); M. Born and Kun Huang, *Dynamical Theory of Crystal Lattices* (Oxford University Press, New York, 1968).

[12] M. Peyrard and S. Aubry, J. Phys. C **16**, 1593 (1983).

[13] O.M. Braun, Yu.S. Kivshar, and I.I. Zelenskaya, Phys. Rev. B **41**, 7118 (1990).

[14] S. Aubry, Physica D **7**, 240 (1983).

[15] H.U. Beyeler, L. Pietronero, and S. Strässler, Phys. Rev. B **22**, 2988 (1990).

[16] O.M. Braun, I.I. Zelenskaya, and Yu.S. Kivshar, Int. J. Mod. Phys. B **8**, 2353 (1994).

[17] O. Braun and M. Peyrard, Phys. Rev. B (to be published).